J. Fluid Mech. (1992), *vol.* 243, *pp.* 15–32
Printed in Great Britain

Numerical simulation of polydisperse sedimentation: equal-sized spheres

By J. M. REVAY AND J. J. L. HIGDON
Department of Chemical Engineering, University of Illinois, Urbana, IL 61801, USA

(Received 14 October 1991 and in revised form 13 February 1992)

This paper describes the results of numerical simulations for polydisperse sedimentation of equal-sized spheres, e.g. particles of different density. Using the Stokesian dynamics algorithm, mobility matrices are computed for random particle configurations and ensemble averages taken to calculate the mean mobility matrices. It is shown that the settling velocities of individual particles species may be expressed in terms of two scalar functions of total volume fraction. These are the self-mobility M_0, ($\sim$ short-time self-diffusion coefficient) and the interaction mobility M_1. This latter quality is related to the velocity of a force-free tracer particle in a suspension of identical particles subjected to a unit force. Numerical values for M_0 and M_1 are calculated for a range of volume fractions from $\phi = 0.025$ to 0.50. All results show excellent agreement with the dilute theory of Batchelor. Simple algebraic expressions are given which well correlate the numerical results.

1. Introduction

The sedimentation of microscopic particles in a fluid suspension is a problem of long-standing interest in fluid dynamics. For particles of uniform size and density, the behaviour of the suspension is relatively well understood and can be characterized by the average settling velocity as a function of volume fraction $u(\phi)$. This velocity is often written in the form $u(\phi) = u^* f(\phi)$, where u^* is the Stokes settling velocity for a single particle $\frac{2}{9}(\rho_s - \rho) g a^2/\mu$ and $f(\phi)$ is a dimensionless quantity called the hindrance function. Comprehensive reviews on the subject of monodisperse sedimentation are given by Batchelor (1972, 1982) and Davis & Acrivos (1985). These authors describe the many experimental, numerical and theoretical studies of sedimentation leading to diverse predictions for the hindrance function f. In addition, they discuss the influence of such features as particle configurations and Brownian forces on the predicted settling rates.

The sedimentation of polydisperse suspensions with particles of varyzing size and/or density is a problem of greater complexity which has not received as much attention. The most obvious difference is that particles of varying type may well have different settling velocities. A rigorous theoretical development for dilute systems has been given by Batchelor & Wen (1982) and Batchelor (1982). Various experimental studies and empirical predictions are discussed by Davis & Birdsell (1988) who conducted experiments on a variety of bidisperse and tridisperse systems. More recently Bruneau *et al.* (1990) measured sedimentation rates in very dilute suspensions showing general agreement with the theory of Batchelor & Wen. The prediction of the individual settling velocities $u_i(\phi_1, \ldots, \phi_N)$ for each of N particle species is an unresolved problem in suspension mechanics.

A surprising feature of polydisperse sedimentation is that suspensions which are

initially uniform may prove unstable leading to strongly non-uniform concentrations in the horizontal plane. These instabilities, first observed by Kynch (1952) appear as fingering phenomena with streams of unequal density. The polydisperse instability has been the subject of numerous experimental studies, by Fessas & Weiland (1981, 1984, and Weiland, Fessas & Ramarao (1984), and has been predicted theoretically by Batchelor & Janse van Rensburg (1986) and by Thiokas (1984, 1986). An alternative theory has been given by Cox (1990). Linear stability theory yields predictions for the onset of instability based on the individual settling velocities $u_i(\phi_j)$ in the unperturbed homogeneous suspension. Thus even in the case of unstable systems, the prediction of the settling functions is the most important problem in polydisperse sedimentation.

Given the difficulty of a theoretical analysis of non-dilute polydisperse sedimentation, we turn our attention to numerical simulation. The most promising approach appears to be the class of algorithms known as *Stokesian dynamics* developed by Brady & Bossis (1985, 1988). This approach has yielded many valuable results for the dynamics of concentrated suspension, including studies of the effective viscosity, the sedimentation rate in monodisperse suspensions and the formation of structure in sheared suspensions.

The Stokesian dynamics algorithm has been used in two classes of simulations. In dynamic simulations, the motion of individual particles is tracked over thousands of time steps. This has the disadvantage that it requires a large computational effort and simulations are limited to small particle samples. On the other hand, the history of the particle motion provides valuable information, not only for average settling rates, but also for detailed statistics on particle configurations and possible structure formation in the suspension.

In contrast to the dynamic simulations, the Monte Carlo algorithms calculate the individual velocities for a given particle configuration and take ensemble averages over many configurations. These algorithms involve less computational effort per particle and may thus be employed with larger sample sizes. The validity of this approach depends on the availability of a collection of particle ensembles which accurately reflects the particle distribution in a real system. In a dynamic simulation, the history of the particle trajectories provides such a collection of samples; however, there is no simple way to generate such a sample *a priori* for an arbitrary system. Under certain circumstances, the sample of particle configurations is well represented by that occurring in classic hard-sphere distributions. Phillips, Brady & Bossis (1988, hereafter referred to as PBB) have used such systems to model monodisperse dispersions, calculating sedimentation rates, effective viscosities and other transport properties. Ladd (1990) has extended the work of PBB to include higher-order representations of the hydrodynamic interactions.

The simulation of polydisperse suspensions is in general far more challenging than that of monodisperse suspensions. Even in the case of a bidisperse suspension, the presence of different particle types will require a larger sample size. In addition, all properties are functions of two independent concentrations ϕ_1 and ϕ_2, as well as parameters such as density ratios, size ratios, etc. These considerations preclude the implementation of large-scale dynamic simulations at this time. As an alternative, we consider Monte Carlo simulations for bidisperse suspensions with a hard-sphere distribution for the particles. This model for the ensemble of particle configurations is quite restrictive for polydisperse suspensions because differences in particle setting rate may affect the pair distribution function. Batchelor (1982) gives a comprehensive discussion of the effect of Brownian diffusion on the particle-pair distribution

function. Briefly, for very dilute systems, the relative motion of identical spheres is zero, hence any amount of diffusion is sufficient to render the pair distribution function uniform. When the relative velocity of particles is non-zero the pair distribution function becomes a function of the particle Péclet number based on this relative velocity. The sedimentation rate is affected not only by the direct action of Brownian forces, but also by the indirect effect on particle configuration. It is only in the asymptotic limit of low Péclet number, $Pe = (u_1^* - u_2^*)\,a/D$ (where a is the particle radius, and D the diffusion coefficient), that we may assume a particle distribution dominated by random Brownian forces. Thus for dilute systems, any results from a random Monte Carlo simulation are strictly valid only in this limit.

For non-dilute systems, the strict validity of the simulation is again confined to low Péclet number. There is, however, some hope that the results may be representative of more general behaviour. As an example, one may compare the settling rate (or permeability) for fixed random versus regularly ordered lattices. In dilute systems, particle interactions given an order-ϕ contribution for the former, but an order-$\phi^{\frac{1}{3}}$ contribution for the latter. At moderate concentrations, however, the settling rates show qualitatively similar behaviour as the ordered versus disordered configuration has less effect on the overall transport properties. In the high concentration, close-packed limits, the effect of particle configuration again becomes significant as it determines the maximum concentration for relative particle motion. The point is simply that idealized particle configurations may provide some insight into the behaviour of systems at arbitrary Péclet number.

Our goal then is to predict the average settling velocities for individual particle species in polydisperse suspensions whose statistical properties may be modelled by an idealized hard-sphere distribution. The individual particle velocities will be computed in a number of uncorrelated configurations to obtain an ensemble average for the settling rates. We restrict our study to spheres of equal size but varying density. As explained in §2, this restriction reduces the computational effort by 2 to 3 orders of magnitude. The velocities are computed using the Stokesian dynamics algorithm as described by PBB. The governing equations and theoretical background are presented in §2, the Stokesian dynamics algorithm in §3, numerical results in §4 and application to polydisperse instabilities is given in §5.

2. Basic formulation

Consider a cubic volume of side L containing a suspension of N spherical particles of radius a_α suspended in a Newtonian fluid of density ρ and viscosity μ. In a given configuration, we denote the particle position by $\boldsymbol{r}_\alpha$ and the particle density by ρ_α. Here, the particles are numbered from 1 to N where we employ Greek subscripts exclusively for particle numbering. Each particle is acted upn by a force $\boldsymbol{f}_\alpha$, but is torque free. While the analysis applies to arbitrary forces, we shall be most interested in gravitational forces for which $\boldsymbol{f}_\alpha = (\frac{4}{3}\pi a^3)(\rho_\alpha - \rho)\,\boldsymbol{g}$. We suppose that the volume is replicated in a periodic manner to form an infinite suspension filling the space. As the number of particles in the cell grows large, the transport properties of the suspension will approach those of an infinite suspension with the same statistical properties.

The governing equations are the Stokes equations and continuity equation for an incompressible Newtonian fluid

$$-\nabla p + \mu \nabla^2 \boldsymbol{u} = 0, \tag{1}$$

$$\nabla \cdot \boldsymbol{u} = 0, \tag{2}$$

with boundary conditions on the particle surfaces $\boldsymbol{u} = \boldsymbol{u}_\alpha + \boldsymbol{\Omega}_\alpha \times (\boldsymbol{r} - \boldsymbol{r}_\alpha)$ at $|\boldsymbol{r} - \boldsymbol{r}_\alpha| = a_\alpha$. The force $\boldsymbol{f}_\alpha$ on each particle is given, and the torque is zero. As noted previously we require periodicity with respect to a cube of side L.

With these specifications, the problem is completely determined and one may in principle solve for the individual particle velocities $\boldsymbol{u}_\alpha$ in terms of the applied forces $\boldsymbol{f}_\alpha$. A brief description of the solution procedure (Stokesian dynamics) is given in the following section. Owing to the linearity of the equations, the velocities may be related to the forces through a mobility matrix $\boldsymbol{M}_{\alpha\beta}$ such that

$$\boldsymbol{u}_\alpha = \left(\sum_\beta \boldsymbol{M}_{\alpha\beta} \boldsymbol{f}_\beta \right). \tag{3}$$

The mobility matrix $\boldsymbol{M}_{\alpha\beta}$ is the most useful characterization of the particle interactions in a sedimenting suspension. To illustrate the relationship between the mobility matrix and the mean settling velocities, let us first consider a monodisperse suspension where each particle is of raidus a acted upon by an identical $\boldsymbol{f} = 6\pi\mu a \boldsymbol{u}^*$. The velocity of a given particle α is expressed

$$\boldsymbol{u}_\alpha = \left(\sum_\beta \boldsymbol{M}_{\alpha\beta} \right) \boldsymbol{f} \tag{4}$$

and the average settling velocity for a particle in this instance is

$$\bar{\boldsymbol{u}} = \left(\frac{1}{N} \sum_\alpha \sum_\beta \boldsymbol{M}_{\alpha\beta} \right) \boldsymbol{f}. \tag{5}$$

If the sample size were sufficiently large, this average settling velocity would approach the same value for all configurations with the same statistical particle distribution. Given the more modest sample size used in a typical simulation, we taken an ensemble average of $\bar{\boldsymbol{u}}$ over many configurations. The average mobility matrix is an isotropic function of volume fraction whose principal value is simply related to the hindrance function defined earlier; that is,

$$\bar{\boldsymbol{M}}(\phi) \equiv \frac{1}{N} \sum_\alpha \sum_\beta \boldsymbol{M}_{\alpha\beta} = \frac{f(\phi)}{6\pi\mu a} \boldsymbol{I}. \tag{6}$$

Next, consider the case of a bidisperse suspension with N_1, N_2 particles of types 1 and 2 respectively. For the moment, these may have arbitrary sizes and forces. Once again, one may solve for the mobility matrix and calculate the average settling rates for each individual species. The individual velocities are expressed

$$\boldsymbol{u}_\alpha = \left(\sum_{\beta \in N_1} \boldsymbol{M}_{\alpha\beta} \right) \boldsymbol{f}_1 + \left(\sum_{\beta \in N_2} \boldsymbol{M}_{\alpha\beta} \right) \boldsymbol{f}_2, \tag{7}$$

and the average velocities are

$$\left.\begin{aligned} \bar{\boldsymbol{u}}_1 &= \frac{1}{N_1} \left(\sum_{\alpha \in N_1} \sum_{\beta \in N_1} \boldsymbol{M}_{\alpha\beta} \right) \boldsymbol{f}_1 + \frac{1}{N_1} \left(\sum_{\alpha \in N_1} \sum_{\beta \in N_2} \boldsymbol{M}_{\alpha\beta} \right) \boldsymbol{f}_2, \\ \bar{\boldsymbol{u}}_2 &= \frac{1}{N_2} \left(\sum_{\alpha \in N_2} \sum_{\beta \in N_1} \boldsymbol{M}_{\alpha\beta} \right) \boldsymbol{f}_1 + \frac{1}{N_2} \left(\sum_{\alpha \in N_2} \sum_{\beta \in N_2} \boldsymbol{M}_{\alpha\beta} \right) \boldsymbol{f}_2 \end{aligned}\right\} \tag{8}$$

for α in sets (1) and (2) respectively.

This is a far more challenging problem. In the first instance, one needs far larger sample sizes and/or far more configurations owing to the two different particle types. Furthermore, if one particle is substantially larger than the other it may take a factor $O(a_1/a_2)^3$ more particles of the smaller 2 type to obtain a reasonable sample. Second, the average settling velocities are functions of two independent variables, and separate average mobility matrices must be computed for each combination of volume fractions (ϕ_1, ϕ_2). Thus each mobility matrix will be significantly harder to compute, more configurations will be needed for each (ϕ_1, ϕ_2) data point and far more points will be needed for $f(\phi_1, \phi_2)$ as opposed to $f(\phi)$.

Owing to these complications, we defer consideration of the most general system to a later time. Instead, we consider a polydisperse suspension of equal-sized spheres acted upon by arbitrary forces, e.g. particles of different density. For suspensions with random particle distributions, the probability of a particle of type i occupying a given position is ϕ_i/ϕ and all positions are equally probable. Thus the mobility matrix is a function of *geometry* only; it is independent of the particle types, and the average mobility matrices are functions only of *total volume fraction* ϕ. With these results, the averaging process is greatly simplified, leading to

$$\left.\begin{aligned} \bar{\boldsymbol{u}}_1 &= \left(\frac{1}{N}\sum_{\alpha} \boldsymbol{M}_{\alpha\alpha}\right)\boldsymbol{f}_1 + \left(\frac{1}{N}\sum_{\alpha}\sum_{\beta\neq\alpha} \boldsymbol{M}_{\alpha\beta}\right)\left(\frac{\phi_1}{\phi}\boldsymbol{f}_1 + \frac{\phi_2}{\phi}\boldsymbol{f}_2\right), \\ \bar{\boldsymbol{u}}_2 &= \left(\frac{1}{N}\sum_{\alpha} \boldsymbol{M}_{\alpha\alpha}\right)\boldsymbol{f}_2 + \left(\frac{1}{N}\sum_{\alpha}\sum_{\beta\neq\alpha} \boldsymbol{M}_{\alpha\beta}\right)\left(\frac{\phi_1}{\phi}\boldsymbol{f}_1 + \frac{\phi_2}{\phi}\boldsymbol{f}_2\right). \end{aligned}\right\} \tag{9}$$

We find it convenient to define the self-mobility matrix $\boldsymbol{M}_0(\phi)$ and the interaction mobility matrix $\boldsymbol{M}_1(\phi)$ as

$$\boldsymbol{M}_0(\phi) = \left(\frac{1}{N}\sum_{\alpha} \boldsymbol{M}_{\alpha\alpha}\right), \tag{10}$$

$$\boldsymbol{M}_1(\phi) = \left(\frac{1}{N}\sum_{\alpha}\sum_{\beta\neq\alpha} \boldsymbol{M}_{\alpha\beta}\right). \tag{11}$$

Each of these matrices is isotropic, and hence is completely characterized by its scalar principal value M_0, M_1 respectively. The self mobility $M_0(\phi)$ represents the average velocity of a particle subject to a unit force in a suspension of force-free particles. This is of course the same (within a scaling factor) as the short-time self-diffusion coefficient, previously computed by PBB, i.e. $D_0^S = kTM_0$. The interaction mobility M_1 represents the average velocity of a force-free tracer particle in a suspension of particles subjected to an identical unit force. With these definitions, the average velocity of species i may be written in the compact form

$$\bar{\boldsymbol{u}}_i = M_0(\phi)\boldsymbol{f}_i + M_1(\phi)\left(\frac{\phi_1}{\phi}\boldsymbol{f}_1 + \frac{\phi_2}{\phi}\boldsymbol{f}_2\right). \tag{12}$$

In fact, this result immediately generalizes to a polydisperse suspension with any number of different particle forces. We simply define the average force

$$\bar{\boldsymbol{f}} = \sum_i \left(\frac{\phi_i}{\phi}\right)\boldsymbol{f}_i \equiv \frac{1}{N}\sum_{\alpha} \boldsymbol{f}_{\alpha}, \tag{13}$$

where the summation is either over particle species i or over individual particles α.

The mean settling velocity for a particle of species i in a polydisperse suspension of equal-size spheres is then written

$$\bar{\boldsymbol{u}}_i = M_0(\phi)\boldsymbol{f}_i + M_1(\phi)\bar{\boldsymbol{f}}. \tag{14}$$

This result is the most important analytical result of the present effort. Combined with the numerical evaluation of the scalar functions M_0 and M_1 as functions of ϕ, it provides a complete description of the average settling velocities for suspensions of equal-sized spheres. For a monodisperse suspension, we found the settling rate is characterized by a single scalar function $f(\phi)$ or $\bar{M}(\phi)$; for the present circumstances the settling velocities may be expressed in terms of two scalar functions of ϕ. Equation (14) is written in terms of M_0 and M_1; however, comparing (6) with (10), (11) we have the simple relationship $\bar{M} = M_0 + M_1$, thus we might just as well employ M_0 and $\bar{M}$ or M_0 and $f(\phi)$.

3. Numerical algorithms

To make use of the formalism in the preceding section, we require a numerical procedure for calculating the global mobility matrix $\boldsymbol{M}_{\alpha\beta}$ for a system of N equal-sized spherical particles. We have chosen to implement the Stokesian dynamics algorithm. This algorithm has been thoroughly described elsewhere, and we shall not repeat the detailed development or justification. A comprehensive discussion is given by Brady & Bossis (1988) and Brady *et al.* (1988) and a description of the specific implementation for Monte Carlo simulations in periodic systems is given by PBB. We shall restrict ourselves to a brief description of the fundamental feature of the method.

Following Brady & Bossis, one may construct a *grand resistance matrix* $\mathscr{R}$ relating the force, torque and stresslet of a particle to the velocity, angular velocity and strain rate:

$$\begin{pmatrix} \boldsymbol{F} \\ \boldsymbol{T} \\ \boldsymbol{S} \end{pmatrix} = -\mathscr{R} \begin{pmatrix} \boldsymbol{U} - \boldsymbol{U}^\infty \\ \boldsymbol{\Omega} - \boldsymbol{\Omega}^\infty \\ -\boldsymbol{E}^\infty \end{pmatrix}. \tag{15}$$

The inverse of this matrix is defined as the *grand mobility matrix*, $\mathscr{M} = \mathscr{R}^{-1}$. In the Stokesian dynamics algorithm the grand resistance matrix is calculated as

$$\mathscr{R} = (\mathscr{M}^\infty)^{-1} + \mathscr{R}_{2B} - \mathscr{R}^\infty{}_{2B} \tag{16}$$

In the first term $\mathscr{M}^\infty$ is an approximation to the grand mobility matrix formed via a far-field multipole expansion. Its inverse includes multibody interactions, and it is by itself a good approximation for widely dispersed particles. The second term $\mathscr{R}_{2B}$ is the exact two-body resistance matrix. The final term is the far-field approximation of the two-body resistance matrix. If particles are far apart, the last two terms cancel and the first gives a good approximation to the resistance matrix. If two particles are close together and well separated from others, the first and last terms cancel and the middle term gives an accurate representation. In cases where many particles are in close proximity, the accuracy will depend on the order of terms retained in the multipole expansions. It is well known that straightforward evaluation of multipole interactions leads to non-convergent sums owing to the strong r^{-1} interaction of the Stokeslets. These sums may be made convergent by a number of techniques as described by PBB. We note that convergence follows automatically in periodic

systems where the singularities and mobility tensors are based on the periodic form of the fundamental solution. Brady & Bossis review a large number of test cases showing excellent results with the force–torque–stresslet (FTS) level algorithm. This is the form adopted in the present effort. Note that the mobility matrix $\boldsymbol{M}_{\alpha\beta}$ required in our study is a submatrix of the grand mobility matrix $\mathscr{M}$ found as the inverse of $\mathscr{R}$.

Given a technique for calculating the mobility matrix, the next step in the method is to generate particle distributions in the periodic box. For low volume fractions ($\phi < 0.25$) particles may be added by sequential random placement in the box. At higher concentrations, however, the probability of finding an open position becomes vanishingly small. To overcome this difficulty, we follow PBB and place all particles in the cell in the initial step. Particles are then subjected to random displacements until their positions are statistically uncorrelated with the initial configuration. Two initial configurations were employed: the particles on a simple cubic lattice spanning the cell or close packed in one corner of the cell. The number of particle displacements was adjusted to achieve linear correlation coefficients $r_c < 0.5$. Good agreement was found with the mean radial distribution function $g(r)$ given by Barker & Henderson (1971). Results were found to be independent of the initial configuration and consistent with sequential random addition at concentrations ($\phi < 0.25$) for which that approach was viable. In all respects, the results of this process were consistent with the experience reported by PBB. At the highest concentrations ($\phi > 0.45$) as many as 10000 attempted moves per particle were employed to ensure uncorrelated samples. We note that the calculation of individual average settling velocities for particle species in bidisperse suspensions was more susceptible to fluctuations than the single settling velocity in monodisperse systems. Thus more configurations were needed to approach a smooth result. This behaviour is consistent with expectations based on the respective definitions of $\overline{M}$, M_0 and M_1. More specifically, because $\overline{M}$ is defined as a double sum over all particles and M_0 is a single sum, one expects smoother behaviour for $\overline{M}$.

4. Numerical results

To demonstrate the accuracy of our Stokesian dynamics alogrithm, a number of numerical tests were performed. First, we calculated the drag coefficient for a configuration of three spheres in an equilateral triangle. These results showed excellent agreement with the analytical solution of Kim (1987) for all separations. Next, we calculated the permeability for a simple cubic lattice of spheres and compared it with the high-order numerical results of Zick & Homsy (1982). Again, excellent agreement was found, consistent with the reports of Brady & Bossis (1988). Based on these results and on the consistency with the results of PBB described below, we conclude that an accurate and reliable implementation of the FTS algorithm was achieved. For further tests and discussion of the algorithm itself, the reader is referred to the review article by Brady & Bossis (1988) and to PBB.

For random hard-sphere suspensions, we calculated the mobility matrices and sedimentation velocities for a range of particle volume fractions from $\phi = 0.025$ to 0.50. Several simulations were performed at each concentration, employing 27, 64 and 100 particles. These computations parallel those of PBB except that those authors used smaller sample sizes up to 64 particles, and most importantly did not calculate M_1. The results for the calculation of the self-mobility M_0 are shown in figure 1. The open symbols showing the result for various sample sizes are consistent

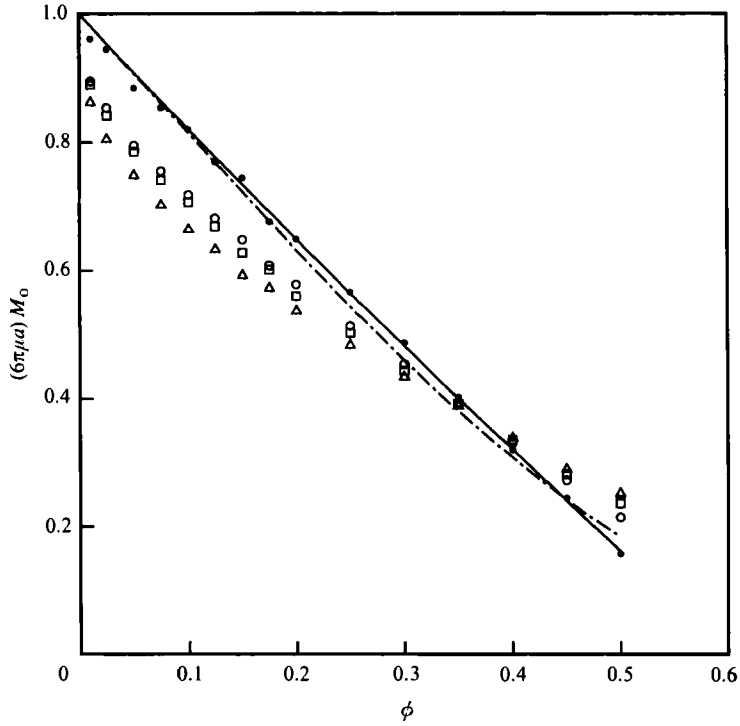

FIGURE 1. Self-mobility M_0 as a function of volume fraction. Number of particles in sample size: △, 27; □, 64; ○, 100; filled circles are extrapolated values for $N \to \infty$. Continuous lines are least-squares curves (17) fit to extrapolated data: ——, present results; — - —, data of Ladd (1990).

with results of PBB (up to their maximum of 64 particles) for the short-time self-diffusion coefficient. The filled circles show the extrapolated values for $N \to \infty$. The extrapolation is based on a simple analysis to correct for the finite size of the periodic system (PBB). At low volume fractions, periodic images of the force on sphere α induce a velocity $O(\phi/N)^{\frac{1}{3}}$. Based on the definition, these images must be subtracted off to obtain the correct value for M_0. In the dilute limit, one may subtract off Hasimoto's (1959) value 1.7601 $(\phi/N)^{\frac{1}{3}}$, or simply extrapolate using the results for $N = 27$, 64, 100 assuming an error $\sim N^{-\frac{1}{3}}$. Each method gives comparable results at low ϕ and both yield results consistent with the low-volume-fraction asymptote $(1-1.83\phi)$ given by Batchelor (1976). At higher volume fractions, the images of the forces are screened by the intervening spheres and the ϕ dependence is modified while the basic $N^{-\frac{1}{3}}$ dependence remains. In this case, one may use Hasimoto's result with a screening correction (Ladd 1990) or use the direct extrapolation method as before. We prefer to rely to direct extrapolation. The solid symbols in figure 1 are computed assuming an $N^{-\frac{1}{3}}$ error at all ϕ. To minimize scatter, the three data sets (27, 64, 100) were fit in a least-squares sense to obtain a single extrapolated value.

For convenience, we have calculated a least-squares fit (as a function of ϕ) for the extrapolated data, matching the intercept and the asymptotic slope at low ϕ:

$$(6\pi\mu a)M_0 = 1 - 1.83\phi + 0.4084\phi^2 - 0.2108\phi^3. \tag{17}$$

This function is shown as the solid line in figure 1. Ladd (1990) simulated sedimenting suspensions using an algorithm similar to that of PBB, but including higher-order multipole expansions. His results are in excellent agreement with the present

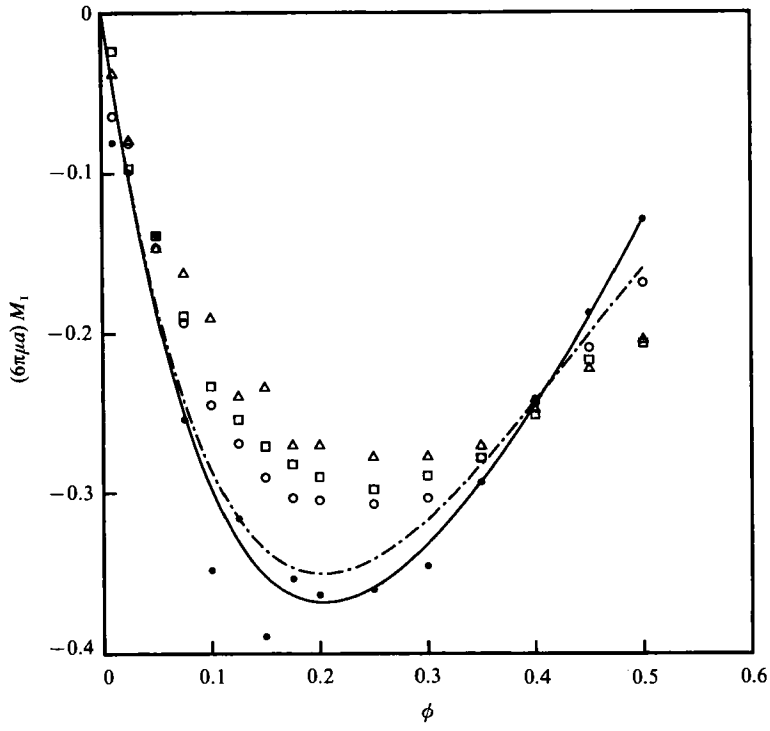

FIGURE 2. Interaction mobility $M_{\rm I}$ as a function of volume fraction. Number of particles in sample size: △, 27; □, 64; ○, 100. Continuous lines are least-squares curve (17), (18) fit to the extrapolated data: ——, present results; — · — ·, data of Ladd (1990).

simulation as shown in figure 1. Both simulations are also consistent with the theoretical prediction of Beenakker & Mazur (1984).

In figure 2 we plot the interaction mobility $M_{\rm I}$ using the same symbol conventions as in figure 1. The asymptotic behaviour for small ϕ (-4.72ϕ) may be inferred from Batchelor's (1972, 1976) results for $M_{\rm O}$ and for $f(\phi) = (1-6.55\phi)$. From its definition, recall that $M_{\rm I}$ is the velocity of a force-free tracer particle in a suspension of particles with identical forces f. Owing to this result, there are no image forces for the tracer particle itself. In a dilute suspension, the periodic image forces of the other particles introduce an error $\sim \phi(\phi/N)^{\frac{1}{3}} \sim \phi^{\frac{4}{3}}N^{-\frac{1}{3}}$. This error does not affect the limiting slope at small ϕ, hence all results show reasonable agreement with Batchelor's asymptotic theory. As before, we extrapolate to $N\rightarrow\infty$ assuming an $N^{-\frac{1}{3}}$ error and show the results as the solid symbols on figure 2. There is substantial scatter in our extrapolated data for $M_{\rm I}$. While the $N = 100$ results are fairly smooth, the $N = 64$, and especially $N = 27$ results are relatively noisy. The solid line shown in figure 2 is the result of a least-squares fit (17), (18) as described below. In computing the latter result, we have arbitrarily excluded the data points at $\phi = 0.10$ and 0.15, which seem excessively affected by extrapolation error. Ladd did not calculate $M_{\rm I}$ explicitly, but the result is easily inferred from his calculations for $M_{\rm O}$ and $f(\phi)$. The resulting curve shown in figure 2 is in excellent agreement with the present results. One might have some reservations about the large magnitude of the $N\rightarrow\infty$ correction. Initially, we had significant concerns about this effect; however, we note that Ladd's extrapolations were of comparable size, and the data he presented are somewhat smoother than our own.

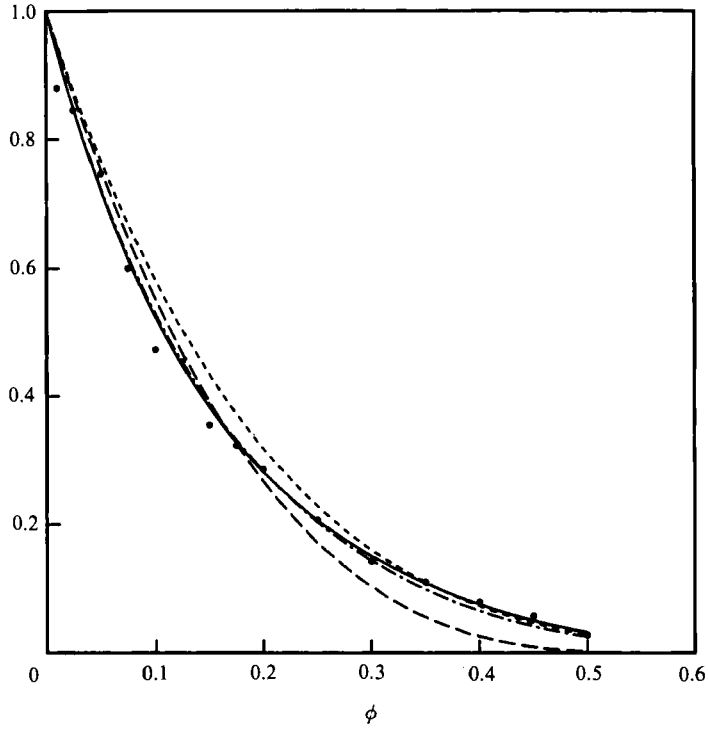

FIGURE 3. Hindrance function $f(\phi) = 6\pi\mu a\overline{M}$ as a function of volume fraction. Theoretical curves based on least squares fit (18): ——, present results; — · —, results of Ladd (1990). Experimental curves recommended by: ----, Garside & Al-Dibouni (1977); – – – –, Buscall *et al.* (1982).

Figure 3 shows the calculated values for the hindrance function $f(\phi) \equiv 6\pi\mu a\overline{M}$ as a function of volume fraction. These values are based on the result $\overline{M} = M_0 + M_1$ using the extrapolated values for M_0 and M_1. As with the individual mobility tensors, these results are in excellent agreement with Batchelor's asymptotic theory for low ϕ. This result is in contrast to PBB who calculated $f(\phi)$ but could not discern sufficient trend in the data to obtain a reasonable extrapolation. If one considers M_0 and M_1 separately, the clean extrapolation of M_0 may be combined with the accurate low-ϕ results for M_1 to obtain the correct asymptotic behaviour. In the present circumstances, the availability of data for $N = 100$ allows a reasonable extrapolation for the M_1 data as well. A least-squares fit to our $f(\phi)$ data yields

$$f(\phi) \equiv (6\pi\mu a)\overline{M} = (1-\phi)^{6.55}(1 + 3.458\,\phi^2 + 8.990\,\phi^3). \tag{18}$$

This function is shown as the solid curve in figure 3. The algebraic function to fit the M_1 data of figure 2 is obtained as the difference $\overline{M} - M_0$ using (17) and (18) respectively. As shown in figure 3, our results are in excellent agreement with those of Ladd, and in reasonable agreement with the experimental curves proposed by Garside & Al-Dibouni (1977) and Buscall *et al.* (1982). We note further that Ladd demonstrated consistency with the theory of Beenakker & Mazur.

In comparing the results of PBB and Ladd for $f(\phi)$, one finds a substantial difference which can be attributed to two factors in the latter effort: the inclusion of higher-order multipoles and the extrapolation for large N. In our implementation, we have included the $N \to \infty$ extrapolation, but retained the FTS-order truncation in the multipole expansion. Given the excellent agreement of our results with those of

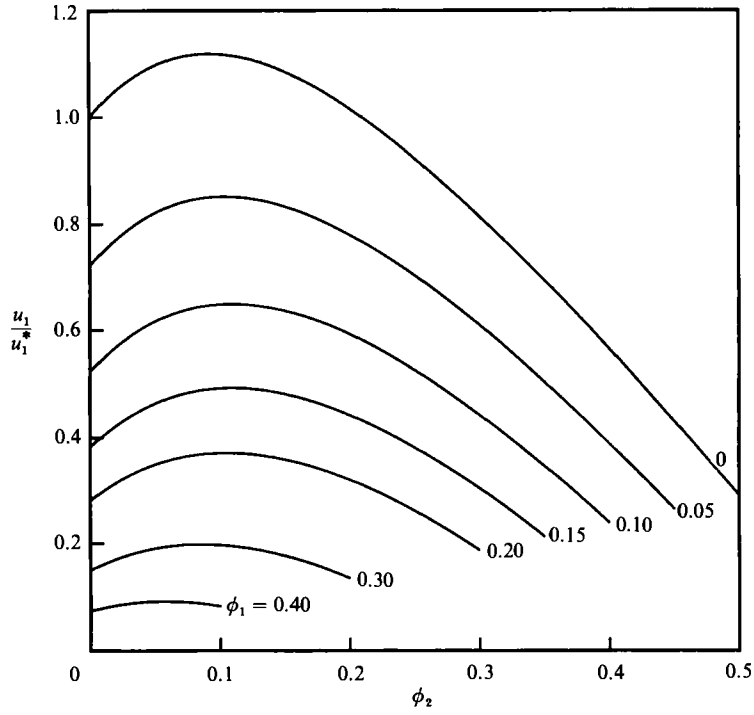

FIGURE 4. Settling velocity u_1/u_1^* as a function of volume fraction ϕ_2 for different values of ϕ_1. Bidisperse suspension with density ratio $\gamma = -1$. Curve labelled 0 is for dilute limit of ϕ_1.

Ladd, we conclude that the effect of finite system size N is the most important limitation of the method. With sufficiently large system sizes, and sufficiently large ensembles to ensure smooth data, excellent results may be achieved with the FTS Stokesian dynamics algorithm.

The algebraic functions (17), (18) combined with the general expression (14) provide predictions for the settling velocities of individual species in a polydisperse suspension of equal-sized spheres. This constitutes the principal result of this paper. To examine further the character of polydisperse sedimentation, we consider some specific examples for bidisperse systems. Following Batchelor, we define the density ratio $\gamma = (\rho_2 - \rho)/(\rho_1 - \rho)$, where ρ is the density of the fluid and ρ_1, ρ_2 are the densities of the respective particle species. Figure 4 shows the settling velocity u_1/u_1^* as a function of ϕ_2 for a suspension with density ratio $\gamma = -1$. By symmetry, the two particle species have identical settling behaviour, with $u_1(\phi_1, \phi_2) = -u_2(\phi_2, \phi_1)$. Each of the curves in figure 4 (for different values of ϕ_1) may be explained as the result of three separate phenomena. First, the addition of small amounts of species 2 will induce a backflow in the overall suspension. For values of $\gamma < 0$, the backflow is in the direction of u_1^* and the settling velocity u_1 increases. Second, as the concentration of species 2 increases, there will be an increase in close encounters between the particle species. This will retard the motion of each species and can result in velocity reversal if one species has a smaller density difference. In figure 4 where the density differences are equal, the close particle interactions counteract the backflow effect, leading to a maximum velocity around $\phi = 0.10$ and monotonic decay thereafter. The third effect is that of hindered settling which reduces the magnitude of all settling velocities independent of direction. This last distinction is somewhat

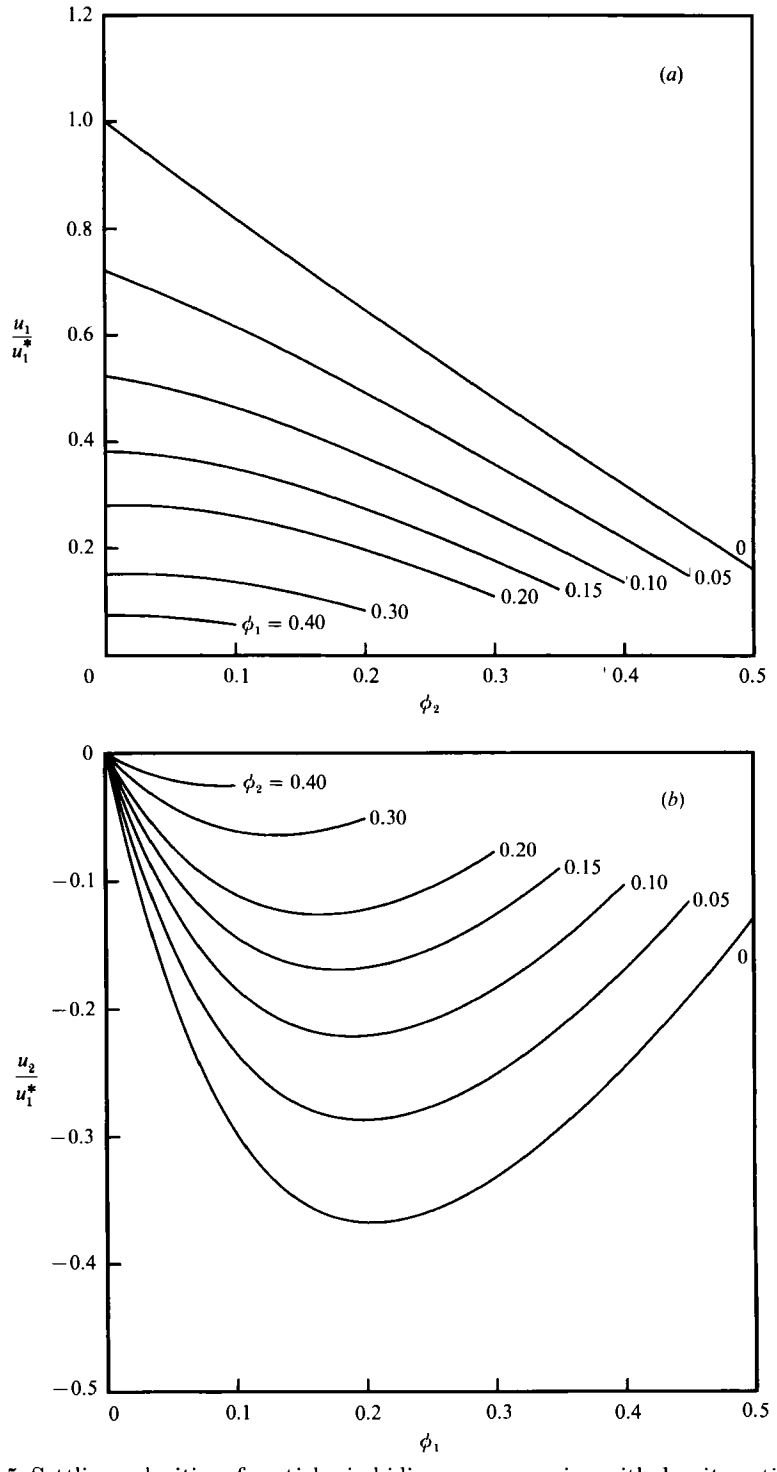

FIGURE 5. Settling velocities of particles in bidisperse suspension with density ratio $\gamma = 0$. Settling velocities non-dimensionalized with respect to dense particle u_1^*. Curves labelled 0 are for dilute limit of respective species. (*a*) u_1/u_1^* as function of ϕ_2 for various ϕ_1. (*b*) u_2/u_1^* as function of ϕ_1 for various ϕ_2.

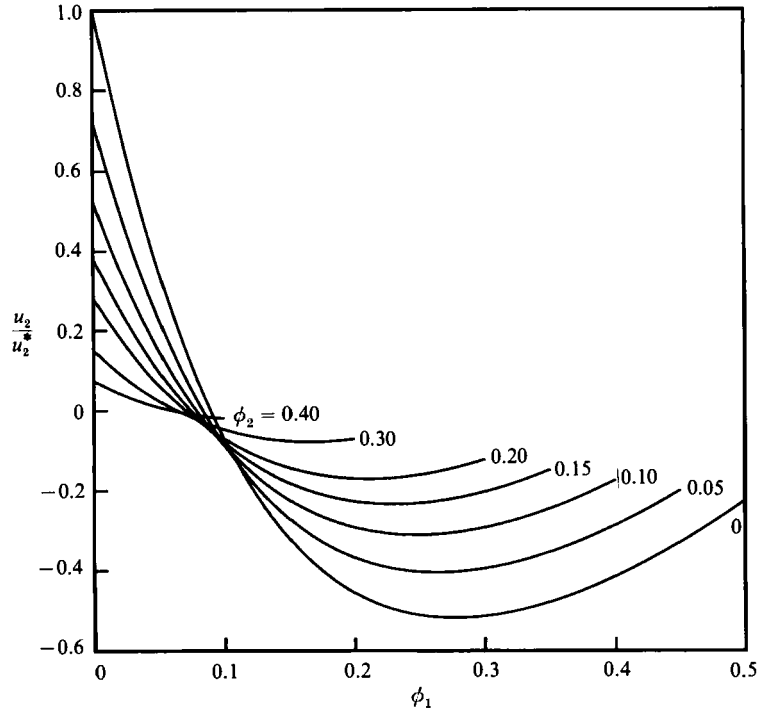

FIGURE 6. Settling velocity u_2/u_2^* as a function of volume fraction ϕ_1 for different values of ϕ_2. Bidisperse suspension with density ratio $\gamma = \frac{1}{3}$. Curve labelled 0 is for dilute limit of ϕ_2.

arbitrary, since backflow and close particle encounters both contribute to the hindered settling effect.

Figure 4 illustrated the case of equal but opposite density differences. Next we set $\gamma = 0$, with species 1 dense, and species 2 neutrally buoyant. The velocities u_1 and u_2 are plotted in figures 5(*a*) and 5(*b*) respectively where each velocity is scaled relative to u_1^*, because $u_2^* \equiv 0$. The behaviour of u_1 is the simplest to explain. There is no backflow effect, and small retardation effect, because species 2 is neutrally buoyant. Thus each curve in figure 5(*a*) shows simple monotonic decay owing to the effect of hindered settling. Figure 5(*b*) is similar to figure 4 in the behaviour it shows. At first, the particle velocity increases, as the neutrally buoyant particles are carried in the backflow of species 1. At higher concentrations of ϕ_1, the close particle interactions counteract the backflow and the velocity decreases; finally, hindrance effects cause a further decrease in the magnitude of the velocity. As the concentration approaches $\phi_{\max} > 0.50$, the self-mobility M_0 would approach zero, and M_1 would cross the axis, becoming positive. In this limit, both particle species would settle at that same rate dictated by $\bar{f}$.

The last example we give is for both species dense with $\gamma = \frac{1}{3}$. The velocity of the denser species u_1 is quite similar to that shown in figure 5(*a*) and is not shown. The velocity of the less-dense species 2 is shown in figure 6. The curves in this figure are influenced by the same factors as those in figure 5(*b*). At low ϕ_1, backflow is the strongest effect and the velocity of the lighter particle decreases rapidly. As close particle interactions become more important, the velocity reaches a minimum and starts to increase. At some $\phi > 0.50$, the velocity will again become positive with both species settling at the same rate.

For particle species with arbitrary density ratios, (14) may be used to produce settling curves similar to those in figures 4–6. A few general trends may be noted. For density differences of opposite sign, $\gamma > 0$, the settling velocity of species 1 (with larger density difference) will lie between the results of figure 4 and figure 5(*a*). There may be some initial increase in settling rate if γ is large enough, but the settling rate will always decrease at larger values of ϕ_2. The settling velocity u_2/u_2^* (of species with smaller density difference) will always increase initially and its behaviour will resemble that shown in figure 4. (Its limiting behaviour will not look like figure 5(*b*) unless we rescale with u_1^*.)

For density differences of like sign, $\gamma > 0$, the settling velocity of species 1 (with larger density differences) will always resemble figure 5(*a*); there will never be any increase in settling velocity. The settling velocity u_2/u_2^* (of species 2 with smaller density difference) will never increase in its original direction, but it may reverse direction and increase in magnitude if the density ratio γ is small enough. The settling curves in the latter case will lie between figures 5(*b*) and 6.

We end this section with a note of caution. These results apply for low-Péclet-number systems where the pair distribution function is independent of the density ratio. The behaviour may be drastically different at high Péclet number, especially for dilute systems. One should consult Batchelor & Wen (1982) for a general discussion of that regime.

5. Instability of bidisperse suspensions

At moderate concentrations, it has been observed that a bidisperse suspension may become unstable if the particles have different settling rates. The criterion for instability given by Batchelor & Janse van Rensburg (1986) and by Thiokas (1986) is

$$\left(\phi_1 \frac{\partial u_1}{\partial \phi_1} - \phi_2 \frac{\partial u_2}{\partial \phi_2} + u_1 - u_2\right)^2 + 4\phi_1 \phi_2 \frac{\partial u_1}{\partial \phi_2} \frac{\partial u_2}{\partial \phi_1} < 0. \tag{19}$$

With the expression for settling velocities and mobilities calculated above, this expression may be evaluated for arbitrary concentration. The neutral stability curves are shown in figure 7. for a number of bidisperse systems with density ratios γ. The dashed lines show buoyant–dense systems ($\gamma < 0$) while the solid lines show dense–dense systems ($\gamma > 0$). For density ratios $\gamma > 0.40$, the suspension is always stable.

As γ increases from -1, one observes a monotonic progression to higher values of ϕ_1 at constant ϕ. This trend may be explained by examining the criterion (19) and the settling curves in figures 4–6. For instability, the second term in (19) must be negative so that the factors $\partial u_1/\partial \phi_2$ and $\partial u_2/\partial \phi_1$ must be of opposite sign, and sufficiently large to offset the first term. For $\gamma < 0$, γ provides the sign change, and the two particles should be in the same relative position on figure 4; that is, both should have positive slope or both have negative slope. If the magnitude of the term is not large enough on the up slope ($\phi_2 < 0.10$) one must jump across the crest, say to $\phi_2 > 0.15$ before the slopes are again of comparable size. At these higher volume fractions, the magnitude of the first term in (19) is decreased and instability sets in. For $\gamma = 0$, $\partial u_1/\partial \phi_2$ is always negative (figure 5*a*) and we look for $\partial u_2/\partial \phi_1$ to be positive. As shown in figure 5(*b*), this first occurs at ϕ_1 greater than about 0.12 and increases as ϕ_2 increases. Values of $\gamma > 0$ are similar to the case $\gamma = 0$, where we again require $\partial u_2/\partial \phi_1 > 0$. From figures 5(*b*) and 6, it is apprent that the concentration ϕ_1 at which this occurs steadily shifts to higher values as γ increases.

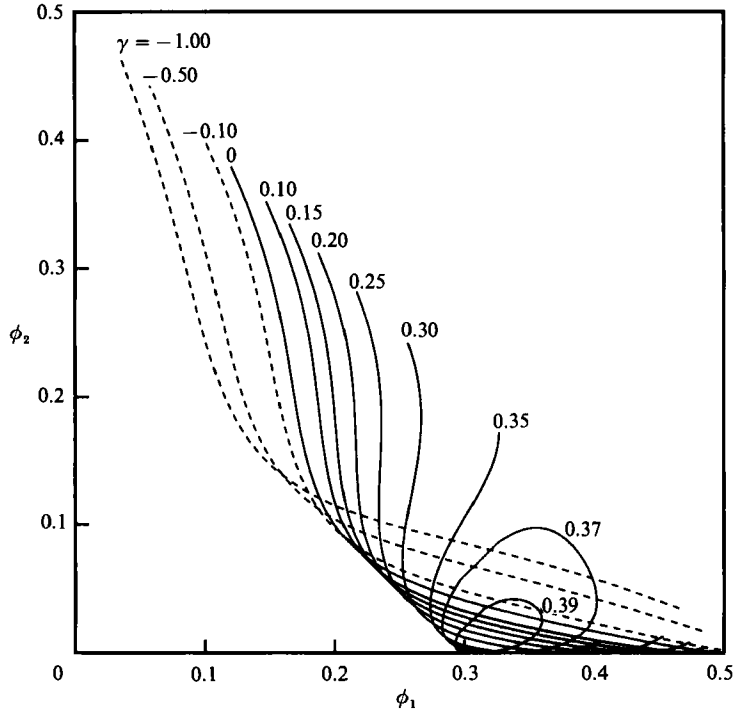

FIGURE 7. Neutral stability curves for the instability of a bidisperse suspension as predicted by (19), for various values of density ratio γ. Dashed lines show buoyant–dense systems ($\gamma < 0$), while solid lines show dense–dense systems ($\gamma > 0$).

A rough comparison with the experimental data of Fessas & Weiland (1981, 1984) and Whitmore (1955) is given in figure 8 for the two cases $\gamma = 0$ (solid circles) and $\gamma = -1$ (open circles). The continuous lines are the respective neutral stability curves from figure 7. The predictions capture the qualitative behaviour quite well but are shifted by approximately 5–10% in volume fraction. There are several factors which might contribute to this discrepancy. First is the fact that Stokesian dynamics algorithm employs a low-order truncation in the multipole expansion and might not be accurately modelling the hydrodynamic interactions for concentrated suspensions. To investigate this possibility, we computed stability curves based on Ladd's mobility results. The curves were qualitatively similar with at most a 1–2% shift in volume fraction over most of the range. The only larger departures occurred for total volume fraction $\phi > 0.45$, which is well above the range of interest. The second factor is the possibility of experimental error, owing to the extreme difficulty in obtaining closely monodisperse-sized particles. We do not believe this factor to be significant for systems with $\gamma < 0$, because even a factor of 2 error in particle velocity (say from $\gamma = -1$ to -0.5) yields a negligible shift in the position of the neutral stability curve.

The third concern, which we feel is the most important, is the fact that experiments were performed at conditions with high Péclet numbers where particle configurations may differ from the hard-sphere distributions used in this paper. It is useful to recall the respective expressions for the settling velocity under dilute conditions (Batchelor & Wen 1982);

low Péclet number $\quad u_1/u_1^* = 1-6.55\,\phi+(-1.83-4.72\,\gamma)\,\phi_2$;

high Péclet number: $\quad u_1/u_1^* = 1-6.55\,\phi+(-2.52-0.13\,\gamma)\,\phi_2$.

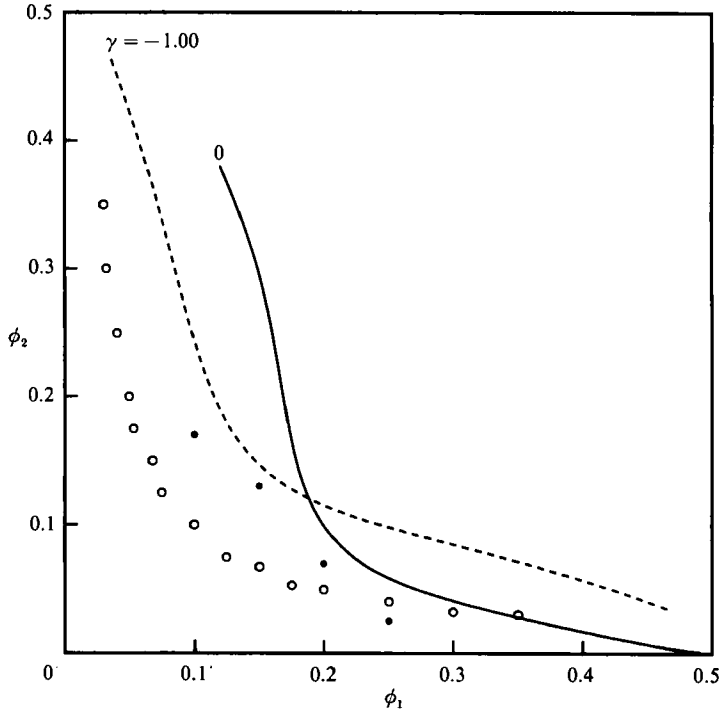

FIGURE 8. Comparison of stability criterion (19) with experiments: ●, neutrally buoyant–dense system $\gamma = 0$, Whitmore (1955); ○, buoyant–dense system $\gamma = -1$, Fessas & Weiland (1981, 1984). The lines are the respective neutral stability curves from figure 7.

The wide variation in the terms proportional to γ, $(-4.72\gamma\phi_2)$ at low Pe and $(-0.13\gamma\phi_2)$ at high Pe, reflects the highly asymmetric particle distribution. At low Pe, the probability of a particle being within a certain distance is independent of the particle type. At high Pe, a particle of different density will interact with a test particle in a brief encounter and then move off, while a particle of the same density will remain in the vicinity until another particle intercepts the pair. For concentrated suspensions, interactions with three and more particles occur more frequently and the like-particle bias may not be as strong. Nonetheless, the dilute results remind us of the importance of the particle distribution in sedimenting suspensions.

Despite the lack of quantitative agreeement, we emphasize that the stability criterion of Batchelor & Janse van Rensburg and Thiokas captures the qualitative behaviour of the bidisperse instability quite well. By contrast, the theory of Cox predicts that bidisperse suspensions are unconditionally unstable for all concentrations and all density ratios. The only exceptions are for particles of widely different size and particles of exactly equal density. Cox notes that his theory requires horizontal perturbations in concentration, while that of BJR requires vertical perturbations. While this is true, it omits an important difference between the theories. Given an arbitrary initial perturbation broken into its component Fourier modes $e^{imx}e^{iny}$, Cox's theory predicts *stability* for all modes except $n = 0$; that is, it requires a perturbation which is non-zero in the mean. Batchelor & Jansen van Rensburg and Thiokas predict *instability* for all m, n except $n = 0$. The simultaneous growth of all modes would lead to a fine-scale graininess in the initial growth phase – exactly as observed in the experiments of Batchelor & Janse van

Rensburg. On balance, we feel that the evidence clearly supports the theory of Batchelor & Jansen van Rensburg and Thiokas. It is very likely that the irreversible particle interactions discussed by Cox are important in the dynamics of the instability, but only in the later stages when macroscopic convective motion ensues.

This work was supported in part by the National Science Foundation. Computational time was made available by the National Center for Supercomputing Applications.

REFERENCES

BARKER, J. A. & HENDERSON, D. 1971 Monte Carlo values for the radial distribution function of a system of fluid hard spheres. *Molec. Phys.* **21**, 187–191.

BATCHELOR, G. K. 1972 Sedimentation in a dilute dispersion of spheres. *J. Fluid Mech.* **52**, 245–268.

BATCHLOR, G. K. 1976 Brownian diffusion of particles with hydrodynamic interaction. *J. Fluid Mech.* **74**, 1–29.

BATCHELOR, G. K. 1982 Sedimentation in a dilute polydisperse system of interacting spheres. Part 1. General theory. *J. Fluid Mech.* **119**, 379–408.

BATCHELOR, G. K. & JANSE VAN RENSBURG, R. W. 1986 Structure formation in bidisperse sedimentation. *J. Fluid Mech.* **166**, 379–407.

BATCHELOR, G. K. & WEN, C. S. 1982 Sedimentation in a dilute polydisperse system of interacting spheres. Part 2. Numerical results. *J. Fluid Mech.* **124**, 495–528.

BEENAKKER, C. W. J. & MAZUR, P. 1874 Diffusion of spheres in concentrated suspension II. *Physica* **126A**, 349–370.

BRADY, J. F. & BOSSIS, G. 1985 The rheology of concentrated suspensions of spheres in simple shear flow by numerical simulation. *J. Fluid Mech.* **155**, 105–129.

BRADY, J. F. & BOSSIS, G. 1988 Stokesian dynamics *Ann. Rev. Fluid Mech.* **20**, 111–157.

BRADY, J. F., PHILLIPS, R. J., LESTER, J. C. & BOSSIS, G. 1988 Dynamic simulation of hydrodynamically interacting suspensions. *J. Fluid Mech.* **195**, 257–280.

BRUNEAU, D., ANTHORE, R., FEUILLEBOIS, F., AUVRAY, X. & PETIPAS, C. 1990 Measurement of the average velocity of sedimentation in a dilute polydisperse suspension of spheres. *J. Fluid Mech.* **21**, 577–596.

BUSCALL, R., GOODWIN, J. W., OTTEWILL, R. H. & TADROS, T. F. 1982 The settling of particles through Newtonian and non-Newtonian media. *J. Coll Old Interface. Sci.* **85**, 78–86.

COX, R. G. 1990 Instability of sedimenting bidisperse suspensions. *Intl J. Multiphase Flow.* **16**, 617–638.

DAVIS, R. H. & ACRIVOS, A. 1985 Sedimentation of noncolloidal particles at low Reynolds number. *Ann. Rev. Fluid. Mech.* **17**, 91–118.

DAVIS, R. H. & BIRDSELL, K. H. 1988 Hindered settling of semidilute monodisperse and polydisperse suspensions. *AIChE J.* **34**, 123–129.

FESSAS, Y. P. & WEILAND, R. H. 1981 Convective solids settling by a buoyant solid phase. *AIChE J.* **27**, 588–592.

FESSAS, Y. P. & WEILAND, R. H. 1984 The settling of suspensions promoted by rigid buoyant particles. *Intl J. Multiphase Flow* **10**, 485–507.

GARSIDE, J. & AL-DIBOUNI, M. R. 1977 Velocity-voidage relationships for fluidization and sedimentation in solid–liquid systems. *Ind. Engng Chem., Proc. Des. Dev.* **16**, 206–214.

HASIMOTO, H. 1959 On the periodic fundamental solutions of the Stokes equations and their application to viscous flow past a cubic array of spheres. *J. Fluid Mech.* **5**, 317–328.

KIM, S. 1987 Stokes flow past three spheres: An analytical solution. *Phys. Fluids* **30**, 2309–2314.

KYNCH, G. J. 1952 A theory of sedimentation. *Trans. Faraday Soc.* **48**, 166–176.

LADD, A. J. C. 1990 Hydrodynamic transport coefficients of random dispersions of hard spheres. *J. Chem. Phys.* **93**, 3484–3494.

PHILLIPS, R. J., BRADY, J. F. & BOSSIS, G. 1988 Hydrodynamic transport properties of hard-sphere dispersions. I. Suspension of freely mobile particles. *Phys. Fluids* **31**, 3462–3472 (referred to herein as PBB).

THIOKAS, J. 1984 The instability of bidisperse suspensions. M.S. thesis, University of Illinois.

THIOKAS, J. 1986 The stability of multiphase suspensions. Ph.D. thesis, University of Illinois.

WEILAND, R. H., FESSAS, Y. P. & RAMARAO, B. V. 1984 On instabilities arising during sedimentation of two-component mixtures of solids. *J. Fluid Mech.* **142**, 383–389.

WHITMORE, R. L. 1955 The sedimentation of suspensions of spheres. *Brit. J. Appl. Phys.* **6**, 239–245.

ZICK, A. & HOMSY, G. M. 1982 Stokes flow through periodic arrays. *J. Fluid Mech.* **115**, 13–26.